

Solar Supergranulation Waves Detected in Surface Doppler Shift

J. Schou

*W. W. Hansen Experimental Physics Laboratory, Stanford University, Stanford, CA
94305-4085*

ABSTRACT

Recently Gizon, Duvall, and Schou (2002) suggested that supergranulation has a wave-like component. In this paper I show that the same phenomenon can be observed using surface Doppler shift data, thereby confirming their observations. I am also able to measure the dispersion relation to lower wavenumbers and to extend the results for rotation and meridional flows beyond $\pm 70^\circ$ latitude.

1. Introduction

Solar supergranulation, which was first described more than 40 years ago by Leighton, Noyes, and Simon (1961), has remained difficult to explain. While it appears to be similar to the granulation, several observations, such as the anomalous flows obtained using correlation tracking or similar methods (e.g. Beck and Schou (2000), in the following BS), challenge the interpretation as a simple convective phenomenon. An alternative explanation is that the supergranulation has a wave-like component and observational evidence for this was recently reported by Gizon, Duvall, and Schou (2002) (GDS in the following).

It has been the cause of some concern that the wave like character has not been observed previously, given the many measurements of the rotation rate of the supergranulation and attempts to determine why it appears to be anomalous. A likely explanation is that it was obscured by the limitations of the surface Doppler shift data.

Supergranular motions are predominantly horizontal near the photosphere. Let V_ϕ be the velocity in the longitudinal (ϕ) direction and V_θ the velocity in the latitude (θ) direction. The observed Doppler velocity V is then given by

$$V = V_\phi \sin \phi + V_\theta \cos \phi \sin \theta \quad (1)$$

under the assumption that the observations are made in the equatorial plane (i.e. that $B_0 = 0$) at a large distance from the Sun. For the V_ϕ component, in particular, the projection leads to a large modulation of the signal as the Sun rotates and to a significant spreading of the power in the frequency domain.

2. Data Analysis and Results

The data used here are the same as those used in BS, which provides further details. They consist of a 60 day sequence of 1024^2 full disk Doppler velocity images obtained by the MDI instrument (Scherrer, et al. 1995) on the SOHO spacecraft, covering the time period 1996 May 24 to 1996 July 22. These images were derotated and averaged to a 60 minute cadence, remapped to a uniform grid in longitude and latitude and binned down to have a resolution of 1200 points covering 360° of longitude and 600 points in latitude between $\pm 90^\circ$. A temporal average was removed as part of this process.

Strips in longitude were extracted, multiplied by a weighting function, tracked at a latitude dependent rate, zero padded to 360° by 12° and passed through a 3 dimensional Fourier transform. The weighting function is a product of a function of θ and a function of ϕ . The function of θ is 1 for $|\delta\theta| \leq 4.5^\circ$, 0 for $|\delta\theta| \geq 5.5^\circ$ and falls off as a cosine bell for $4.5^\circ \leq |\delta\theta| \leq 5.5^\circ$, where $\delta\theta$ is the distance from the target latitude. Two weighting functions in ϕ were applied. One is optimized for recovering V_ϕ , the other for recovering V_θ . The first weighting function is given by $W_\phi = A_\phi \text{sign}\phi / \sqrt{\sin^2 \phi + 0.01}$, where A_ϕ is an apodization function which is 0 for $|\phi| = 0^\circ$ and for $|\phi| > 80^\circ$, 1 for $10^\circ < |\phi| < 70^\circ$ and cosine bell apodized for $0^\circ < |\phi| < 10^\circ$ and $70^\circ < |\phi| < 80^\circ$. The second weighting function is given by $W_\theta = A_\theta / \sqrt{\cos^2 \phi + 0.01}$, where A_θ is only apodized between 70° and 80° . The small bias of 0.01 was added to avoid singularities.

Figure 1 shows the power as a function of direction of propagation. Note that there is significantly more power in the prograde than in the retrograde direction, consistent with the findings of GDS. Also there is little power in the N-S direction where GDS did observe significant power. Since the method used by GDS is sensitive to both components of the velocity this indicates that the displacement, at least at the surface, is almost entirely in the direction of propagation.

Given the above waves in the ϕ direction should show modulation given by A_ϕ when using the W_ϕ weighting and waves in the θ direction should be modulated by A_θ when using W_θ . For other directions the modulation is more complex and only waves propagating near the longitude and latitude directions are studied here. The velocity projection also means that waves traveling in latitude are essentially unobservable at the equator. At high latitudes the foreshortening becomes a problem.

Figure 2 shows examples of the resulting power spectra. Note the different power level in prograde waves (lower right) and retrograde waves (upper right) in the left panel. In the right panel there is excess power in the southbound waves (upper right) relative to the northbound waves (lower right).

The advection of a wave pattern will, at a given azimuth, lead to two peaks in the power spectra at frequencies $\omega_{\pm} = \pm\omega_0(k) + kv$, where $\omega_0(k)$ is the mode frequency, k is the wavenumber (given here in terms of the equivalent degree $l = kR_{\odot}$, where R_{\odot} is the solar radius) and v is the component of the velocity in the direction of propagation.

To quantify the properties of the waves, power spectra at selected k were extracted and a model consisting of two Lorentzians and a background

$$M(\omega) = \frac{A_-}{1 + \left(\frac{\omega - \omega_-}{w}\right)^2} + \frac{A_+}{1 + \left(\frac{\omega - \omega_+}{w}\right)^2} + B, \quad (2)$$

was fitted to them using a maximum likelihood algorithm. Here A_{\pm} are the amplitudes, w is the the (common) width of the modes and B is a constant background. The dispersion relation may be derived as $\omega_0 = (\omega_+ - \omega_-)/2$ and the flow velocity from $v = (\omega_+ + \omega_-)/2k$. To account for the projection factor and the finite observation time, the model is convolved with an estimate of the appropriate window function.

The power spectra are binned by a factor of 5 in k_x , rebinned to a uniform grid in k and azimuth and directions within $\pm 15^{\circ}$ of the desired direction are averaged before being fitted. This averaging ensures that the log of the resulting power spectra is close to normally distributed with a uniform variance, allowing for a simple maximum likelihood algorithm and stable fits. The inaccuracy in the parameters caused by the averaging over azimuth is negligible.

Figure 3 shows the dispersion relation for the waves traveling in longitude at the equator. The solid line shows the fit of a power law over the interval $50 \leq l \leq 200$, which gives an exponent of 0.56. Points below $l \approx 30$ have proven difficult to fit and may be unreliable.

Figure 3 also shows the rotation rate at the equator, which is almost independent of l , allowing the results to be averaged over l , as done in Figure 4, which also shows the meridional flows.

Finally Figures 5 and 6 shows the amplitude, linewidth and anisotropy.

3. Discussion

Possibly the main result is to confirm the results of GDS. Given the differing analysis techniques this represents a significant confirmation and lays to rest the concerns based on the fact that the phenomenon had not been observed previously in surface Doppler shift data.

While not physically motivated it is interesting that the frequencies appear to follow a square root quite well. As can be seen from Figure 3 the dispersion relation at 40° is quite similar to that at the equator in both directions.

The small variation of the rotation rate with l is consistent with a simple depth independent flow. This is in stark contrast to the numbers derived from the same data in BS, which varied by 10nHz between $l=50$ and $l=200$, and which were difficult to explain. The rotation rate derived here is remarkably close to the magnetic tracer rate of Komm, Howard, and Harvey (1993). The similarity may be related to the fact that the advection of the small magnetic elements appear to be influenced by the supergranulation. This similarity is quite unlike the results in BS, in which the rotation rate, at least at low l , exceeded that of the plasma at any depth. This lends further credence to the idea that the flows inferred here represent physical advection rates.

The meridional flow results appear to be reliable to at least $\pm 70^\circ$ latitude with a clear turnover between 20° and 30° and no sign of a second cell. Note that the meridional flow is not perfectly antisymmetric across the equator. As shown this is largely explained by a P angle error caused by the misalignment of the MDI instrument on the SOHO spacecraft (Toner 2000) and by the difference between the Carrington elements and the true rotation axis of the Sun (Giles 1999). An error in the rotation axis causes part of the rotation velocity to be misidentified as meridional flow.

Figure 5 shows that the power peaks around $l = 100$, as previously seen. The linewidth appears to be an increasing function of l , possibly indicating that smaller scale features damp more quickly. The increase for $l \leq 50$ is likely an artifact of the difficulty in fitting low degree features.

As in GDS Figure 6 shows that the power is highly anisotropic at all latitudes and that the anisotropy is in the prograde direction and increasingly towards the equator at higher latitudes.

The physical nature of these waves, if that is indeed what they are, is still unknown. However, with the results presented here, it may be possible to further constrain the models.

Further progress may be possible by extending these results over time or by probing the depth structure using time-distance helioseismology.

REFERENCES

- Leighton, R. B., Noyes, R. W., and Simon, G. W. 1961, ApJ, 135, 474

- Gizon, L., Duvall, T. L. Jr., and Schou, J. 2002, astro-ph/0208343
- Beck, J. G. and Schou, J. 2000, *Sol. Phys.*, 193, 333
- Giles, P. 1999, PhD Dissertation, Stanford University
- Toner, C. 1999, Private Communications
- Komm, R. W. and Howard, R. F., and Harvey, J. W. 1993, *Sol. Phys.*, 145, 1
- Scherrer, P. H., et al. 1995, *Sol. Phys.*, 162, 129

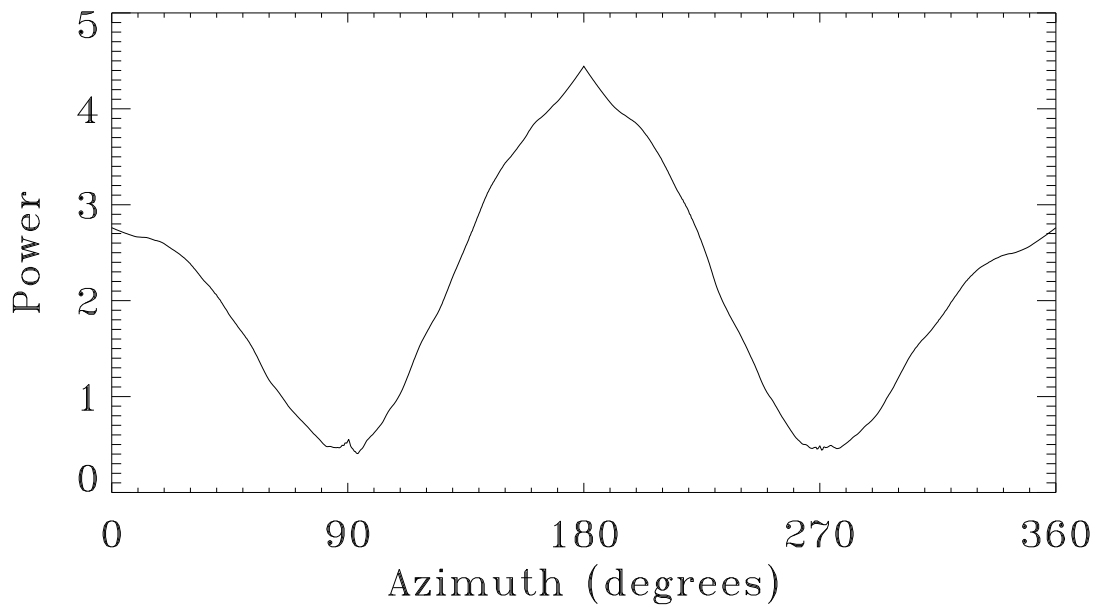


Fig. 1.— Power (averaged over $30 \leq l \leq 200$ and $0 < \nu \leq 10\mu\text{Hz}$) at the equator as a function of azimuth using the W_θ weighting. Prograde is at 180° while northward is at 270° .

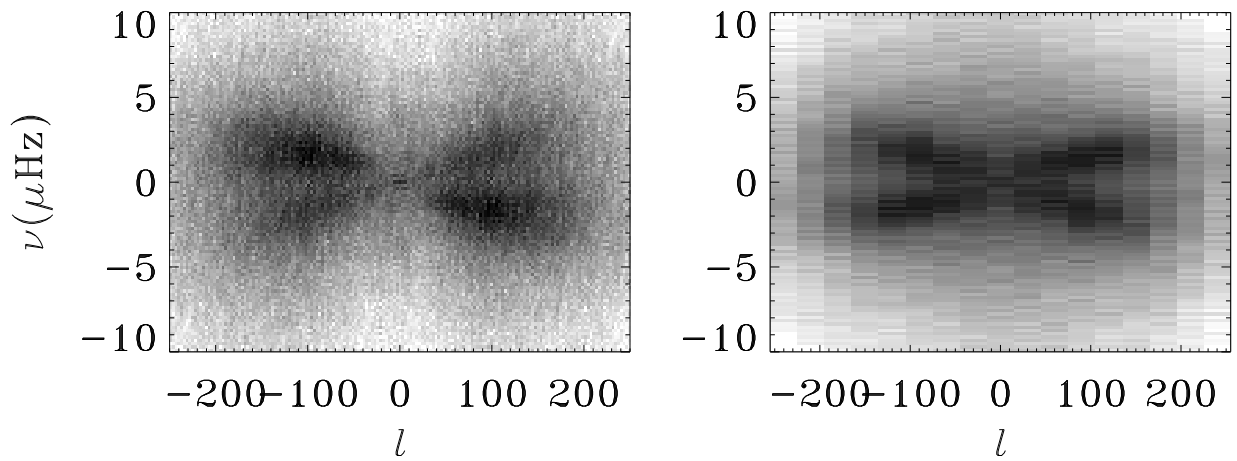


Fig. 2.— Left: Cut in a 3 dimensional power spectrum using W_ϕ at the equator around $k_y = 0$. The grayscale is logarithmic with black 300 times the power of white. Right: Cut at 40° latitude around $k_x = 0$ using W_θ . The poor resolution is due to the narrow strips in latitude. The power is symmetric with respect to a simultaneous change of sign of l and ν .

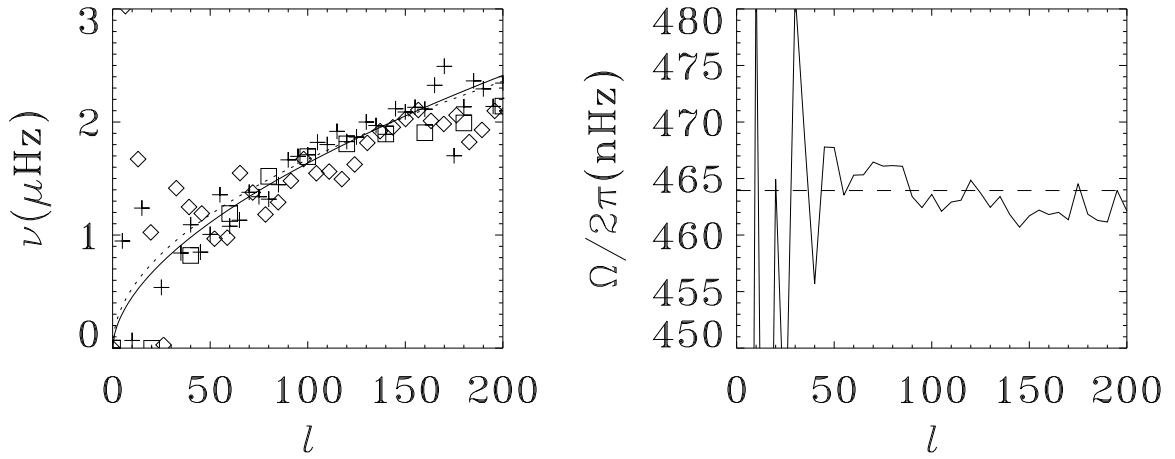


Fig. 3.— Results for waves traveling in longitude at the equator. Left: The dispersion relation (plusses), $1.18(l/50)^{0.5}\mu\text{Hz}$ (dotted) and $1.11(l/50)^{0.56}\mu\text{Hz}$ (solid). Also shown are the results at 40° for waves traveling in longitude (diamonds) and in latitude (squares). The results at high l are less reliable due to the foreshortening. Given the poor resolution in k_x (see Fig. 2) only the results at every 20 in l are shown for the waves traveling in latitude. Right: The sidereal rotation rate (solid) and the equatorial rate from Komm, Howard, and Harvey (1993) (dashed).

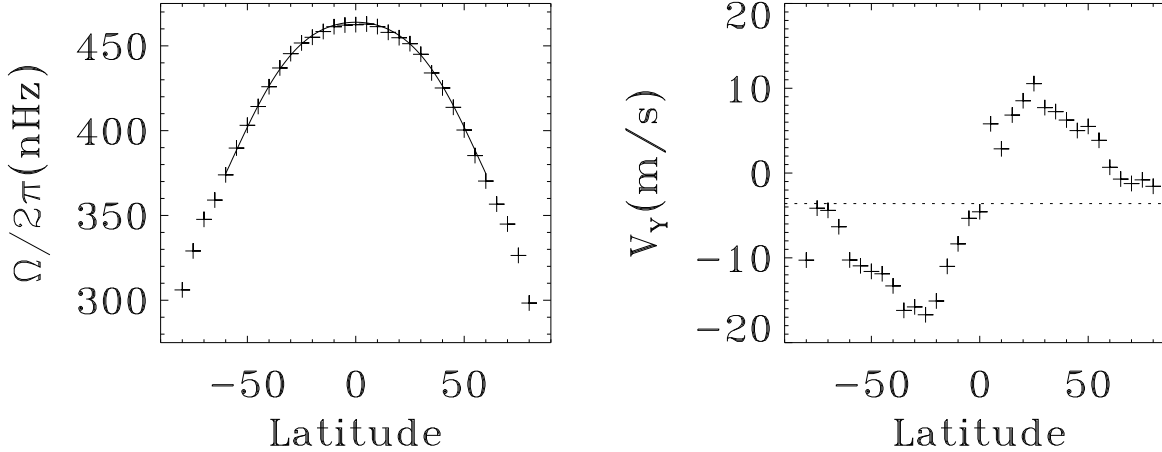


Fig. 4.— Derived flows averaged over $100 \leq l \leq 200$. Left: The sidereal rotation rate derived using W_ϕ (plusses) and the rotation rate from Komm, Howard, and Harvey (1993) (solid). Right: The meridional flow (plusses) (using W_θ) and an estimate of the effect of the incorrect P-angle (dotted).

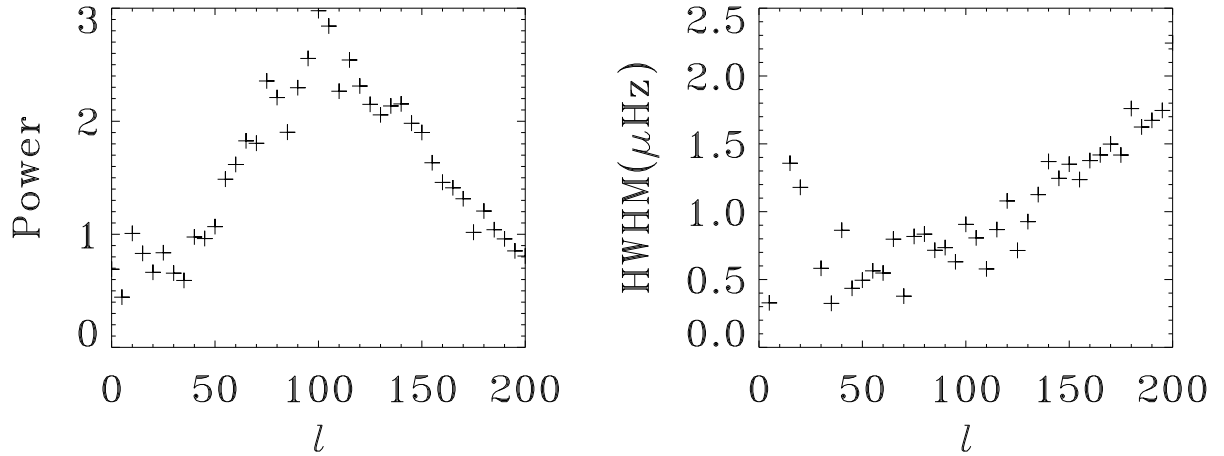


Fig. 5.— Power $w(A_+ + A_-)/2$ and linewidth w as a function of l for longitudinally traveling waves at the equator.

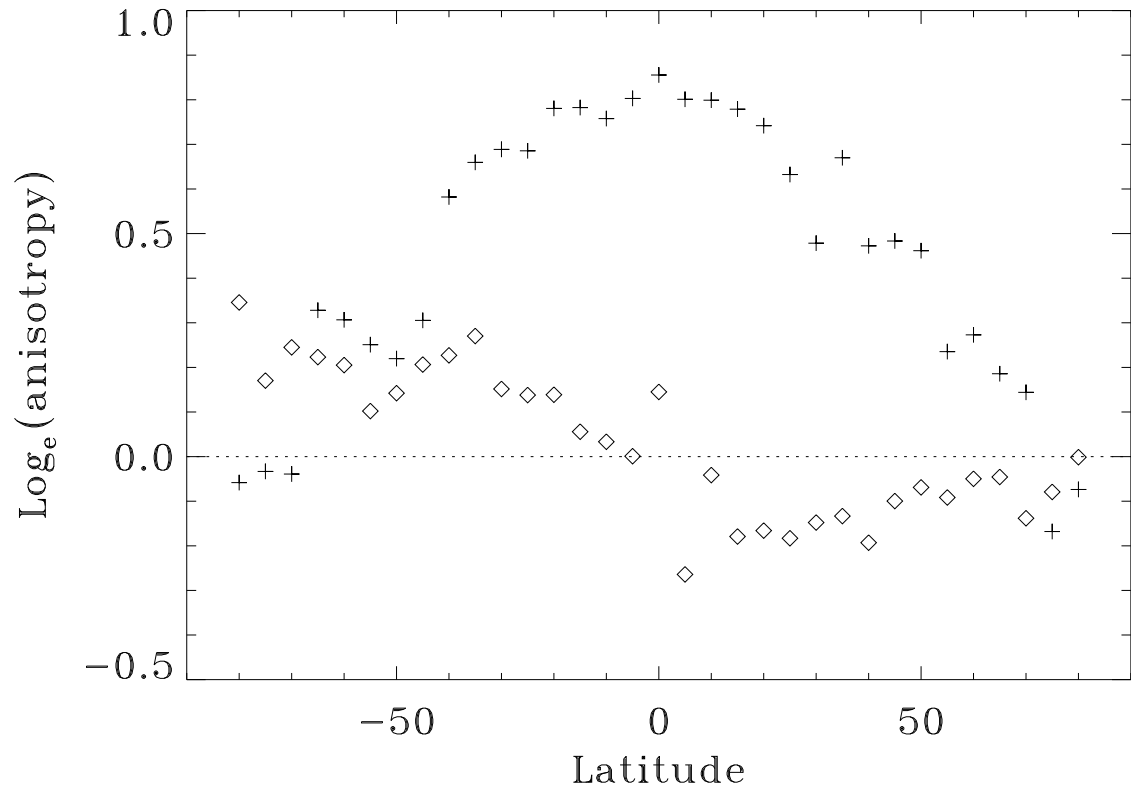


Fig. 6.— Anisotropy as a function of latitude averaged over $100 \leq l \leq 200$. Plusses show the ratio of prograde to retrograde power. Diamonds show the ratio of Northbound power to Southbound power. The anisotropy is essentially independent of l .